

# Hyperspectral Detection Algorithms for Fat-Tailed Clutter

C. A. Steer and M. Bernhardt  
Waterfall Solutions, Parklands,  
Guildford, Surrey GU2 9JX.

## Abstract

*Vegetation backgrounds present a significant challenge to accurate target detection. The distributions of these backgrounds are fat-tailed and have significant weight in the precise probability regions in which targets are expected to reside. Using a novel approach several detection-enhancing factors have been found. These use three different concepts: the transformation of hyperspectral data to a Gaussian distribution; the multi-modal nature of the background clutter distribution; and the scale-invariance of natural spatial correlations. A review is presented of advances related to novel anomaly detectors that utilise these concepts.*

Keywords: Hyperspectral, detection, anomaly, target, clutter

## Introduction

Previously, a novel approach to the design of anomaly detection algorithms was developed [1,2] as part of the Electromagnetic Remote Sensing (EMRS) Defence Technology Centre (DTC) project being reported here. Key to the novelty of the approach was the use of simple generative models to simulate background clutter and the exploitation of lessons learned through phenomenology studies. This approach has been successfully applied to the problem of anomaly detection in vegetation clutter backgrounds in hyperspectral data cubes, and the progress achieved in the last year in this regard forms the basis of this paper.

Several important factors that affect the detection ability of an automatic algorithm have been studied using this approach. These are:

1. The non-Gaussian nature of the vegetation background data.
2. The abundance distribution variability.

3. The nature of vegetation spatial correlations.

The insight into the non-Gaussian statistics of natural backgrounds led to the development of novel anomaly detection algorithms via two different approaches. The first approach was to design completely new algorithms better suited to the actual statistics of the real data, and the second approach was to modify the data rather than the algorithm. In the second case, all data was transformed into a Gaussian as this distribution is assumed by most anomaly detection algorithms.

The second two factors affecting detection performance are motivated by many generative models developed earlier in the project and extensive phenomenology studies [1-4]. Two sources of abundance distribution variability have been identified, namely: spectral and spatial variability. Prior to this project it was not known whether spectral or spatial variability was the dominant factor in degrading detection performance. Spectral variability arises from the intra-class variability of each

material. On the other hand, spatial variability is due to the local vegetation growth and gives rise to characteristic spatial correlations with a highly inhomogeneous abundance distribution.

The spatial correlations of vegetation in hyperspectral imagery are particularly interesting [5-7]. During this project generative models were devised to reflect the physical growth processes present in the natural environment. The result of these and other studies showed that the spatial correlations of vegetation are scale-invariant. In order to take advantage of this property, a class of multi-resolution anomaly detectors was designed and is reported here.

### The Non-Gaussian Nature of Hyperspectral Data

The non-Gaussian nature of hyperspectral data lies at the heart of this project. In order to study hyperspectral pixel distributions a phenomenology tool was developed. This tool has the ability to analyse spatial correlations in imagery and to test whether the data is Gaussian or fat-tailed (i.e. higher probability values far from the mean). A screen-shot of the tool is presented below.

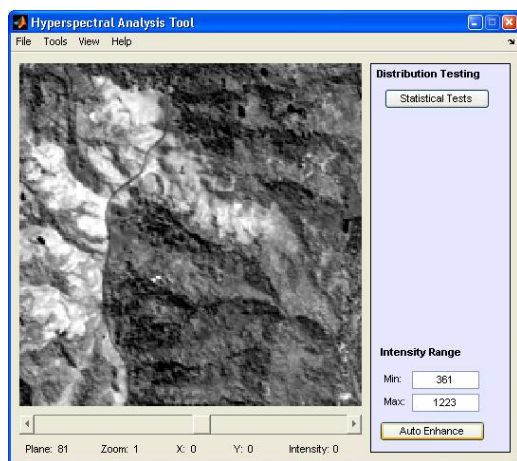


**Figure 1** A screen-shot of the *Hyperspectral phenomenology tool*.

During the course of this project no vegetation background clutter was found to

be Gaussian, or even elliptically contoured (a larger family of functions which encompasses the Gaussian distribution). A test for an elliptically contoured distribution was developed under this project which consisted of a mapping to a hypersphere surface. Under this mapping Gaussian data appears uniform, whereas real data shows distinct structure [2].

The lack of isotropy on the surface of this hypersphere was used to devise a new anomaly detection algorithm. This technique, known as the directional detector, utilises the directional dependence of real data to define a strangeness measure for each pixel. This measure is related to the number of angular neighbours on the surface of the hypersphere. The directional detector was compared to the RX algorithm and example results are presented in Figure 2. It can be seen that even for hard targets for which RX generates large numbers of false-alarms, the directional detector generally has a false-alarm rate of around 5%.

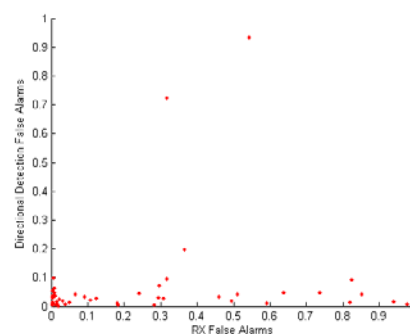


**Figure 2** The number of false alarms of the directional detector against the number of false alarms produced by RX.

Another method for improving the performance of RX is to transform the data from the original fat-tailed distribution to a Gaussian. This is a novel application of the ‘memoryless’ nonlinear transform (MNLT) [8] to hyperspectral data. The MNLT is defined by:

$$\int_x^{\infty} P_{Gaussian}(x) dx = \int_y^{\infty} P_{Data}(y),$$

where  $P_{Data}(y)$  is the empirical pixel distribution and  $P_{Gaussian}(x)$  is a Gaussian distribution. The effect of this can be seen in Figure 3 where the original image and distribution are shown in the top row and the transformed data is shown in the lower row. The resultant MNLT-RX algorithm gave a large improvement in detection ability [4], especially for more challenging targets.

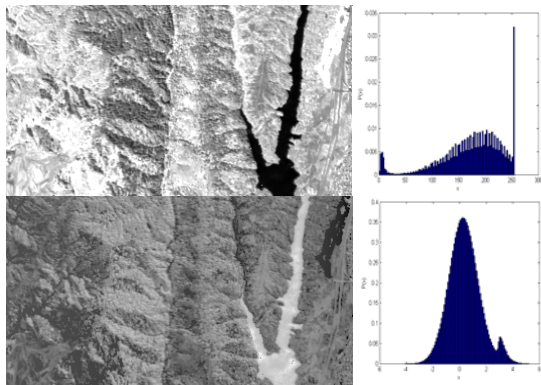


**Figure 3** The effect of the MNLT on non-Gaussian hyperspectral data.

### Variability in Vegetation Abundance Distributions

Spectral variability in vegetation was studied using the high-fidelity simulation tool CAMEO-SIM. Synthetic data cubes were generated based on two spectral libraries, one with many more synthetically generated materials than the other. The synthetic materials library was augmented to give additional variability for each material class. In addition, to generalise the results further these data cubes were rendered using six different atmospheres. In all, twelve different versions of the same scene were generated for each abundance map. Targets were also embedded within the data cube so that degraded detection performance due to spectral variability could be characterised.

Typical receiver operator characteristic (ROC) curves are presented in Figure 4 where the green lines indicate the synthetic material library and blue lines indicate the original spectral library. It can be seen that, on average, spectral variability does not affect the algorithm performance and that a greater factor is atmospheric variation. This evidence also suggests that spatial variability affects detection more than spectral variability.

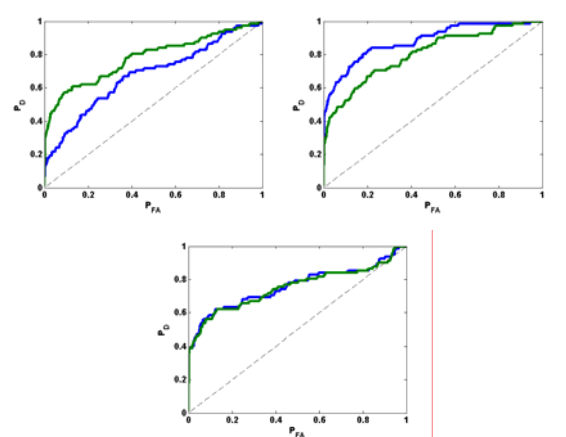


**Figure 4** Typical ROC curves using the RX anomaly detector for different atmospheres.

Spatial variation of vegetation gives rise to a multi-modal background distribution due to the different species present in a scene. In order to reflect this multi-modality a clustering step was performed on the data prior to RX. These Cluster-RX detection algorithms apply RX to each cluster of the hyperspectral data. Two new anomaly detectors based on this principle have been developed. One of these algorithms (IC-RX) clusters using the principal component and another (MC-RX) uses the Mahalanobis distance image. Also, as a baseline algorithm for these cluster-RX methods, a K-means clustering step was also studied [3-4]. The resulting improvement in performance (see [3] for a full report) was significant. This provided strong evidence that the multi-modal nature of vegetation backgrounds is a highly significant factor in degrading algorithm performance.

## Utilising Vegetation Spatial Correlations

Images of natural scenes possess scale-free spatial correlations [5-7]. There is also experimental evidence that such spatial correlations have also been observed in hyperspectral data cubes [1-2]. Therefore, a method which distinguishes hyperspectral features according to their scale or size should help to discriminate man-made and naturally-occurring objects.

In order to identify data cube features according to size, a multi-scale anomaly detection framework was developed. This was based on a pyramidal decomposition and enabled strangeness to be calculated with respect to different image scales.

The newly developed framework consists of three stages. The first stage performs principal component analysis on the whole data cube in order to reduce the number of bands. The second stage decomposes each band into several images of different resolution and the third applies the anomaly detector to each. For the RX algorithm this results in a Mahalanobis map for each resolution image.

Using this framework a number of useful algorithm properties can be demonstrated. These are:

1. It is possible to improve the speed of detection algorithms by using lower-resolution images in place of the original cube.
2. This method can be used to find the target's size.
3. The algorithm is size-selective.
4. Detection ability can be optimised if the size of targets is known *a priori*.

### Algorithm Speed Considerations

All of the algorithms developed under the project have been devised to be

computationally efficient and able to be implemented in real-time on non-specialist hardware.

The multi-resolution framework requires further consideration regarding its real-time implementation because of the numerous design options it offers. These include the number of down-sampling operations performed, the size of the filtering kernel employed and whether or not higher-resolution images are discarded in the process. Speed can be optimised by only using a small kernel and low-resolution images, but a negative impact on detection performance was anticipated and therefore investigated.

Figure 6 shows the ROC curves calculated for the RX algorithm implemented within the multi-resolution framework. The blue, green, red, cyan, purple and yellow coloured lines correspond to successive half-resolution images. The targets were specifically chosen to be highly visible in the full-resolution image. For the smallest targets, this approach blurs the targets very quickly and no significant detection occurs on any other scales. For the larger 16x16 targets this is not the case.

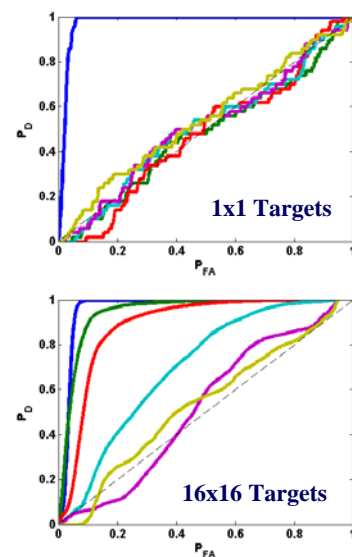


**Figure 6** ROC curves for single and multi-pixel targets using the multi-resolution RX anomaly detection algorithm.

## Estimating Target Size

Once the ROC curves have been produced and the targets are visible, it has been found that the area underneath the ROC curve as a function of resolution provides a good estimate of the target size. The resolution level at which this area goes to half of its original value (i.e. where the algorithm is as good as random guessing) corresponds to the feature scale.

In order to estimate the target size, the ROC curve detection areas were calculated and are presented in Figure 7. As expected, targets cannot be detected based on their spatial extent once their resolution is below that of the image. In the figure 'pyramid level' refers to the number of times the original image size has been halved.

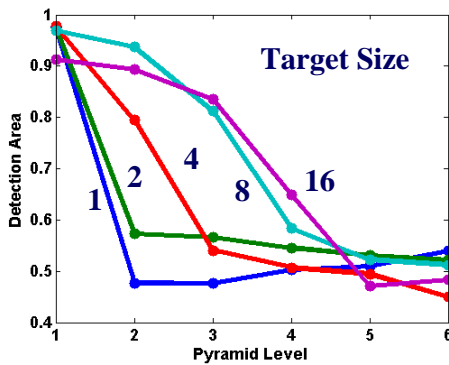


Figure 7 The detection area as a function of synthetic target size and resolution

## Size Selectivity

In order to illustrate the principle behind size selectivity of the multi-resolution detection framework, a synthetic target data set was generated with mixed 4x4 and 16x16 targets. Using the above characterisation of the ROC curve response as a function of image resolution, the difference between the original image and half-size image was used to find anomalies of 4x4 pixels.

The target map is presented in Figure 8 for these two selections. In this figure, red pixels indicate false alarms, green pixels indicate undetected target pixels and yellow pixels indicate detected target pixels. It can be seen in Figure 8 that the choice of using the difference between image resolutions preferentially detects 4x4 targets (shown yellow) but not 16x16 targets. Therefore, this approach allows tuning of the algorithm based on *a priori* target size information.

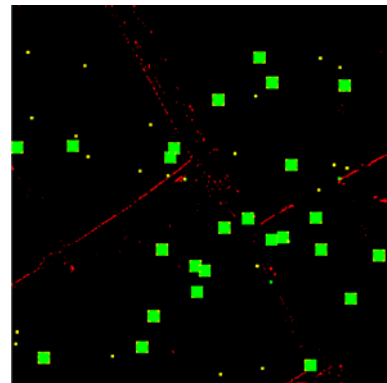
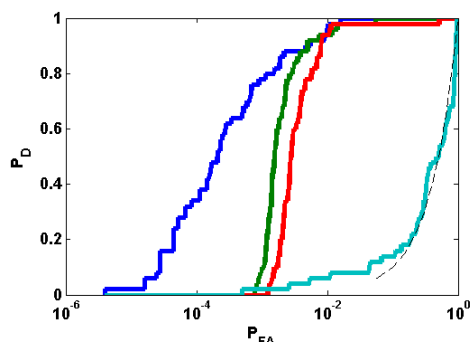


Figure 8 Detected & undetected targets plus false alarms for the multi-resolution plain-RX algorithm.

## A Comparison of Cluster-RX and Multi-Resolution RX Anomaly Detection

Another important research topic that has been ongoing throughout this project is the determination of which natural effects dominate the detection ability of algorithms. Prior to the development of the multi-resolution framework, it had been thought that the biggest degrading effect on detection ability was the multi-modal nature of hyperspectral data because the best detection performance had been obtained using cluster-RX detection algorithms [3-5].



**Figure 9** A comparison of cluster-RX and multi-resolution detection algorithms for single pixel targets.

The ROC curves for the cluster-RX and multi-resolution RX algorithms are presented in Figure 9 for relatively difficult synthetic single pixel targets (10% embedding strength). Cluster-RX results are shown in red, cyan and green (red is IC-RX, cyan is MC-RX, green is K-Means RX) and size optimised multi-resolution RX detector results are shown in blue. The dashed line is the result that would be achieved through random guessing. It can be seen that the size-optimised multi-resolution RX anomaly detector out-performs the cluster-RX methods. This suggests that the use of multi-resolution anomaly detection methods is as important as reflecting the multi-modal character of the vegetation background distribution.

It is the next logical step to reflect both multi-modality and scale-invariance properties into a single anomaly detection algorithm.

## References

1. Waterfall Solutions. Internal Report WS/EMRS/WP1, October (2004).
2. Bernhardt, M., Heather, J., and Watkins, O., Proc. SPIE. **5573**, 215, (2004).
3. Waterfall Solutions. Internal Report WS/EMRS/WP3, March (2006).

4. Waterfall Solutions. Internal Report WS/06/EMRS/HS/TR004, October (2006).
5. Turiel, A., Mato, G., Parga, N., and Nadal, J-P., Phys. Rev. Lett. **80**, 1098, (1998).
6. Torralba, A., and Oliva, A., Network: Comput. Neural Syst. **14**, 391, (2003).
7. Ruderman, D. L., Network: Comput. Neural Syst. **5**, 517, (1994).
8. Tough, J. A., and Ward, K. D., J. Phys. D: Appl. Phys. **32**, 3075, (1999).

## Acknowledgements

The work reported in this paper was funded by the EMRS DTC, established by the UK Ministry of Defence and run by a consortium SELEX Sensors and Airborne Systems, Thales Defence, Roke Manor Research and Filtronic.